ARMY RESEARCH LABORATORY

Induction Heating of Carbon-Fiber Composites: Electrical Potential Distribution Model

by Bruce K. Fink, Roy L. McCullough, and John W. Gillespie Jr.

ARL-TR-2130

November 1999

19991126 090

Approved for public release; distribution is unlimited.

DTIC QUALITY INSPECTED 4

The findings in this report are not to be construed as an official Department of the Army position unless so designated by other authorized documents.

Citation of manufacturer's or trade names does not constitute an official endorsement or approval of the use thereof.

Destroy this report when it is no longer needed. Do not return it to the originator.

Army Research Laboratory
Aberdeen Proving Ground, MD 21005-5069

ARL-TR-2130 **November 1999**

Induction Heating of Carbon-Fiber Composites: Electrical Potential Distribution Model

Bruce K. Fink
Weapons and Materials Research Directorate, ARL

Roy L. McCullough and John W. Gillespie Jr.
University of Delaware

Approved for public release; distribution is unlimited.

Abstract

Mechanisms of heat generation and distribution in carbon-fiber-based composites subjected to an alternating magnetic field are considered. A model that predicts the strength and distribution of these heat sources in the plane of the cross-ply laminate configurations has been developed and verified. In this analysis, the fibers in a cross-ply pair are treated as a grid of conductive loops in the plane. Each such conductive loop uses the alternating magnetic field to produce a rotational electromotive force that induces electric fields in the polymeric regions. Induced electromagnetic energy is converted into thermal energy through dielectric losses in polymeric regions between the carbon fibers in the adjacent orthogonal plies that the conductive loops comprise. Each possible conductive loop is accounted for, and the resulting superposition of potential differences at the nodes leads to the in-plane profile of the electric field in the polymeric regions. Data from AS4 graphite-reinforced polyetheretherketone (PEEK) laminate surface temperature measurements using liquid crystal sheets compare qualitatively with the theory.

Table of Contents

INTENTIONALLY LEFT BLANK.

List of Figures

Figure		Page

1. Introduction

With the advent of advanced thermoplastic-based composites, much research has been directed to take advantage of their unique postprocessing attributes. Thermoplastic resins are stable high molecular weight polymers that retain their chemical identity during processing. Since the fully polymerized thermoplastic resins do not form cross-linked networks, they can be softened and reformed. Alternating magnetic fields provide a localized, noncontact, and expedient source of heating.

It has been established [1] that the primary mechanism of heating in continuous-fiber laminated systems, such as AS4/polyetheretherketone (PEEK) carbon/thermoplastic, is primarily due to dielectric losses in the polymer. This was shown to be true as long as dielectric breakdown did not occur in the polymer. This "local theory" of heating established the mechanism by which electromagnetic energy is converted into heating in the locality of the fiber-fiber intersection, as shown in Figure 1.

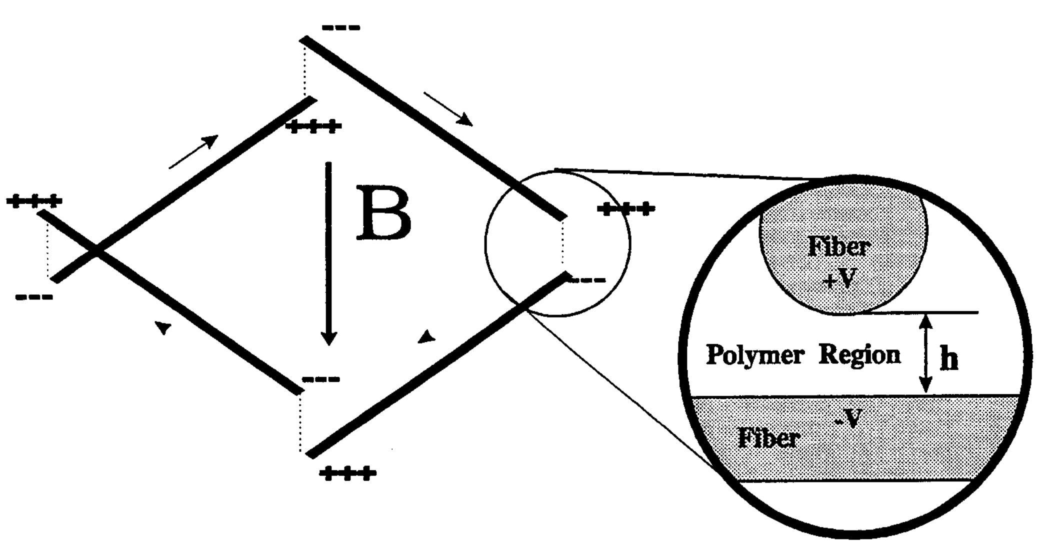

Figure 1. Induced Current Due to a Transverse (Normal to the Plane) Magnetic Field in a $[0/90]_s$ Cross-Ply. A Matrix-Rich Region of Thickness h Exists Between the orthogonal plies in such a laminate.

The local theory provides the basis for a "global model" of heat generation in continuous-fiber cross-ply laminated composite systems. A global model is needed to determine the value of the alternating electric field across the fiber-fiber intersection in all interfiber polymeric regions in order to quantify the distribution of overall heating in the specimen. The global model [2] consists of three additional independent submodels: (1) a fiber layer submodel to analyze the through-thickness electromagnetic response in the composite, (2) a thermal submodel to determine the surface transient thermal response, and (3) the planar grid submodel presented here to describe the in-plane response.

In order to correlate the local theory of heating occurring due to electrical potential differences between intersecting fibers with a compatible model of thermal generation in the plane, the laminate is modeled as an electrical network of intersecting conductors with some reasonable mesh size. For example, Figure 2 shows the electrical network analog associated with a 5×5 grid size representation. The objective of this work is to characterize the interaction between adjacent orthogonal or off-axis plies in the composite laminate subjected to a transverse alternating magnetic field. The model developed to determine this two-dimensional ply-ply interaction is termed the planar grid model to describe its use of a finite grid to represent the plane of the laminate specimen. The interaction between individual fibers through the thickness of the laminate is reported elsewhere.

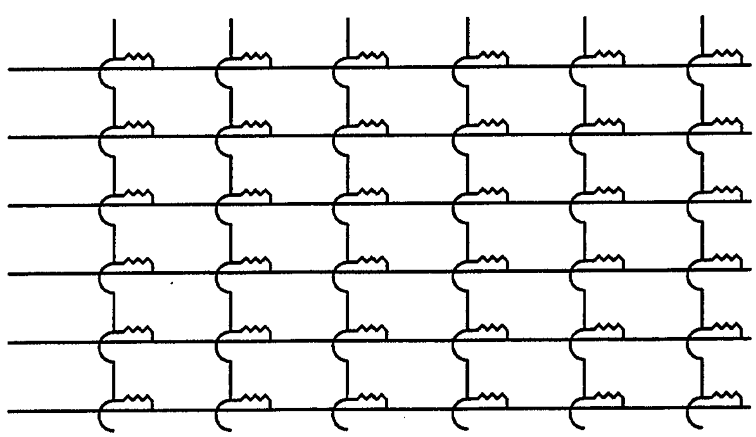

Figure 2. An Electrical Network Analog to a [0/90] Cross-Ply With a 5×5 Grid Size Representation in the Plane. Note That Fiber-Fiber Intersection Resistances Are Considered to Be Equivalent in the Ply-Ply Interaction Submodel.

2. Formulation of Planar Grid Model

Several effects are considered in this analysis. These include

(1) cancellation of electric fields in internal loops,

(2) determination of least-resistive path with respect to matrix-rich intersections,

(3) determination of least-resistive path with respect to fibers, and

(4) incorporation of current density effects

These items, superimposed, provide a view of the planar heating pattern through the distribution of the electric fields along the various conductive paths. The planar grid model incorporates items 1, 2, and 3. Item 4 would account for the possibility of parallel fibers within the same ply randomly coming in contact so that current would have the option of taking several paths in accordance with the effective resistances of the various paths. Such effects would only perturb the distribution of electric fields within a few fiber diameters. Accordingly, these effects are not considered. As a consequence of this simplification, a relatively coarse grid can provide reasonable estimates.

The cancellation of linear electric fields in internal conductive loops is a key element of the model. The applied alternating magnetic field induces a rotational electric potential field about each possible conductive loop, regardless of the loop's effective resistance. A square grid, such as that in Figure 2 and in cross-ply laminates illustrated in Figure 3, can be divided into many possible conductive loops of various shapes and sizes. The minimum number of intersections, however, is four. Three-sided paths are not possible since two interacting unidirectional plies can only form four-sided and greater paths when viewed normal to the plane. In consideration of item 2, the least-resistive path will generally be a path consisting of the minimum number of intersections. The resistance of the fiber lengths has been shown to be negligible compared to

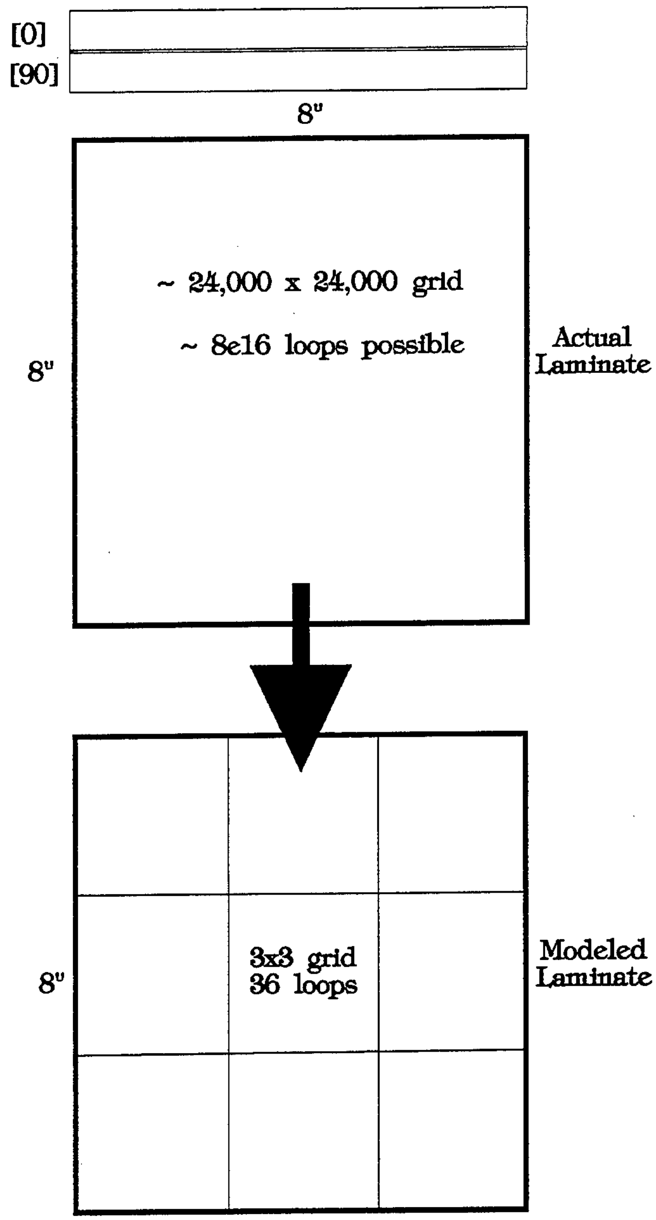

Figure 3. Comparison of Laminate Configuration to a Representative Planar Grid in the Ply-Ply Interaction Submodel.

the resistance of the intersections so that the lengths of the paths traveled are inconsequential (item 3) when considering the path resistance.

An algorithm has been developed that incorporates all possible four-cornered loops in any given grid and calculates and superimposes the induced potentials. Figure 3 shows the actual laminate configuration considered and a representative planar grid model. Note that, in the laminate, there are approximately 24,000 fiber rows in each 20.3-cm-wide (8 in) ply, which combine to make up approximately 8×10^{16} loops. The model assumes an $n \times n$ grid (where n is some small integer) consisting of $1/4\ n^2(n + 1)^2$ possible four-cornered loops. The model of Figure 3 illustrates a 3×3 grid representation, containing 36 possible four-cornered loops. For each possible loop (which consists of four fiber lengths and four matrix regions), the following operations are performed.

(1) Calculate the planar rotational electric potential field (emf) from Faraday's law:

$$\varepsilon = -A\frac{dB}{dt},$$

where is the area of the loop and the time derivative of magnetic field vector **B** is the product of the angular frequency and the scalar B.

(2) Convert the rotational emf for each loop to a directional electric field vector along each fiber length, which comprises the loop, by dividing the emf by the loop perimeter in accordance with

$$\varepsilon = \oint \vec{E} \cdot d\vec{l}\,.$$

(3) Sum the electric fields from all loops for each fiber segment (grid element) obtained from each loop calculation (steps 1 and 2).

(4) Calculate the alternating potential differences across each node in the plane.

Step 4 provides the "nodal" potential difference between fibers in adjacent plies. A separate model is needed to determine how the "layers" of fibers through the thickness interact with their counterparts in the adjacent orthogonal (or off axis) ply. This through-thickness model is described in Fink [2]. The planar grid model can, however, be further analyzed with the realization that it predicts the qualitative nature of heating in the plane of the laminate since heating through dielectric losses [1] is directly proportional to the square of the potential difference:

$$W_j = \frac{\beta_j V_j^2}{h}, \tag{1}$$

where W_j is the heat generation at some node j; β_j is a function of several material, environmental, and microstructural properties at node j; V_j is the potential difference between the fibers at node j; and h is the distance through which the electric field created by V exists, as defined in Figure 1.

Although the voltages cannot be directly measured (due to the high frequency) or the existence of the electric fields directly proven, their manifestation as surface temperature gradients can be observed. Parametric studies were performed verifying the convergence of the grid size to low n values at various coil-to-specimen size ratios and coil locations. Experimental studies verify the location of thermal extremum in the plane, as predicted by the algorithm.

3. Model Predictions

Figure 4 shows an outline of a computer program, which performs the operations described previously. Data representing the input magnetic flux from the coil through each smallest unit loop in the grid (each element) are input to the algorithm. Equation (2) is an example input matrix representing the 5 × 5 grid of Figure 2, with a centered coil superimposed. Since the Helmholtz-type coil that was used in the experimental work provides a uniform distribution of flux in the plane, the contribution of total flux to each grid loop or element can be calculated.

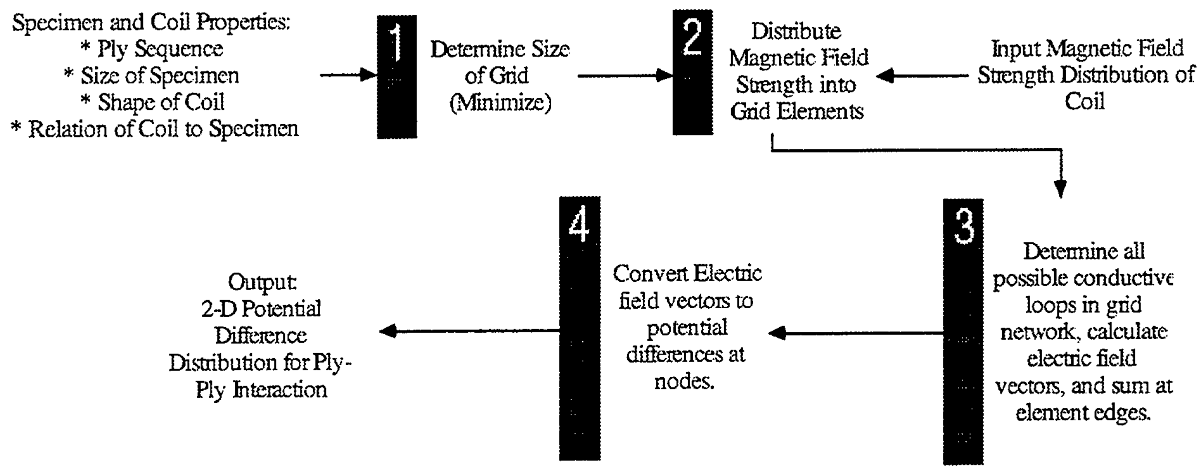

Figure 4. Process Flow Diagram for Planar Grid Model.

Figure 5 shows the 5×5 grid representation superimposed on a square laminated cross-ply specimen with a Helmholtz-type coil centered on the specimen. The placement of the coil determines the area within which the alternating magnetic flux acts normal to the surface. If each element of the modelled grid has a unit area, those elements that are completely enclosed by the magnetic flux field [e.g., element (3,3) in Figure 5] are considered to have a unit flux. Other cells may be only partially influenced by the flux field and have proportionate fractions of the unit flux assigned to them in amounts equivalent to the proportionate fraction of element area covered by the homogeneous flux field. Figure 5 shows these fractions for the example under consideration.

Next, the algorithm normalizes these values so that the total imposed magnetic flux is a unit value. These values are then used as input as shown in equation (2):

$$\text{Input} = \begin{bmatrix} 0 & 0 & 0 & 0 & 0 \\ 0 & 0.036 & 0.143 & 0.036 & 0 \\ 0 & 0.143 & 0.284 & 0.143 & 0 \\ 0 & 0.036 & 0.143 & 0.036 & 0 \\ 0 & 0 & 0 & 0 & 0 \end{bmatrix}. \tag{2}$$

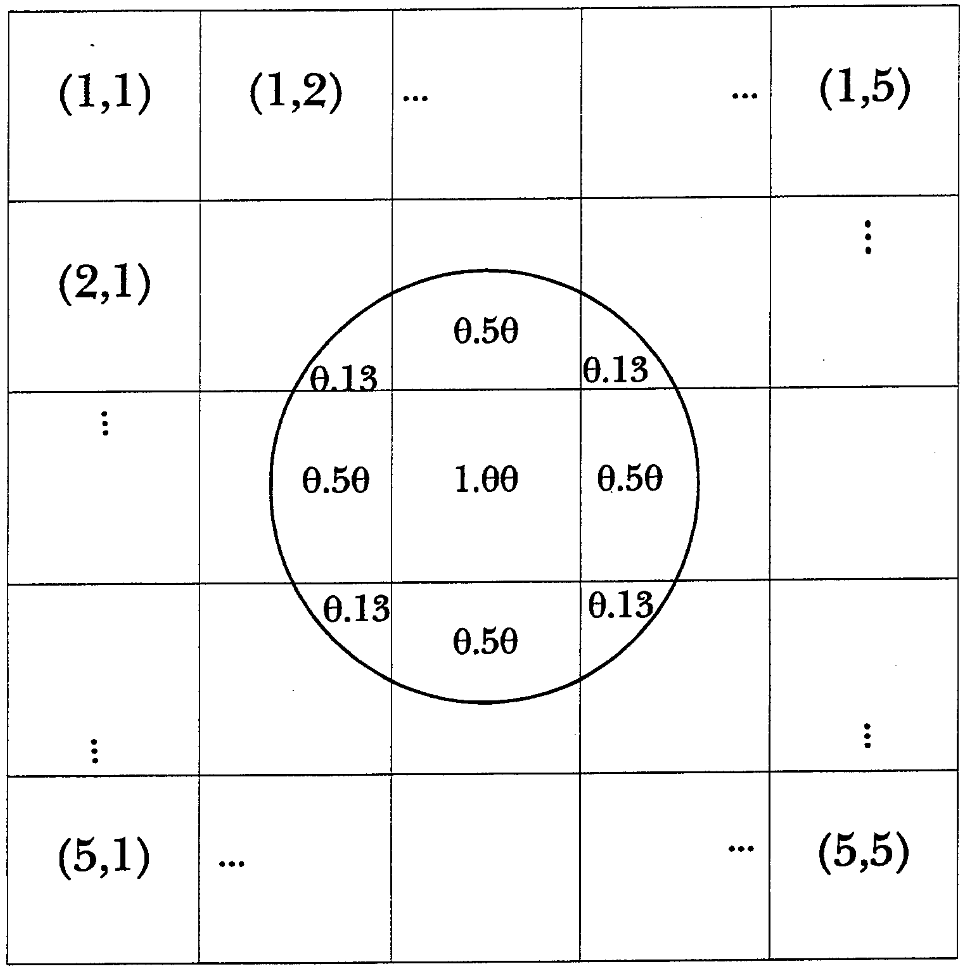

Coil Diameter = One-half Plate Width
Coil Area = 14.2% Plate Area

Figure 5. A 5 x 5 Grid Representation Showing the Distribution of Unit Cell Magnetic Flux. Note That Element (3,3) Has a total Flux Input of Unity.

Note that the sum of all the elements in the input matrix, equation (2), is unity. The code returns the output (nodal voltage per unit magnetic flux) per equation (3) and is displayed in Figures 6 and 7.

Note in equation (2) that the coil was centered on the specimen so that the diagonal plot of Figure 7 provides an avenue for comparison with other centered-coil (i.e., symmetrical coil placement) examples:

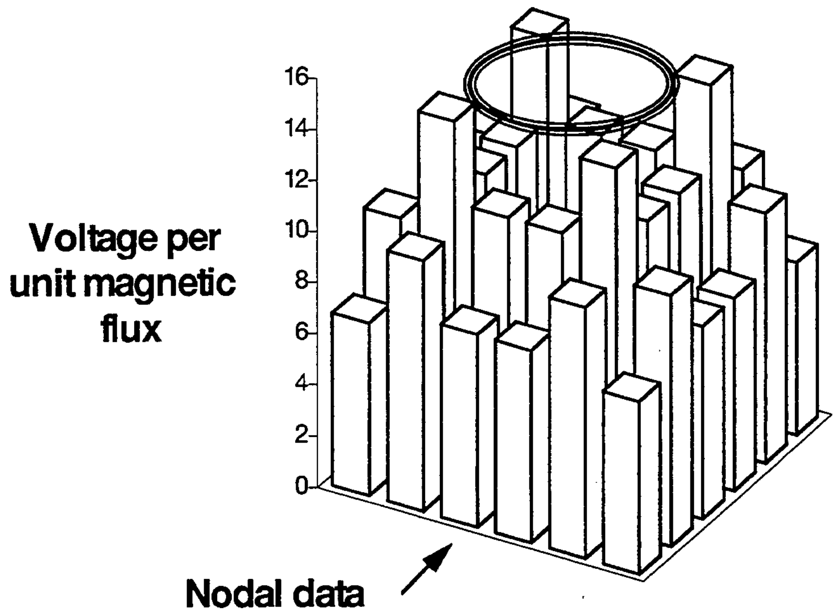

Figure 6. Columnar Plot of Equation (2) for the Output of the Planar Grid Model's Computer Code. Each Column Represents the Voltage Between Plies for a Planar Grid Node in the Plane of the Laminate. The Relative Position of the Coil Is Shown.

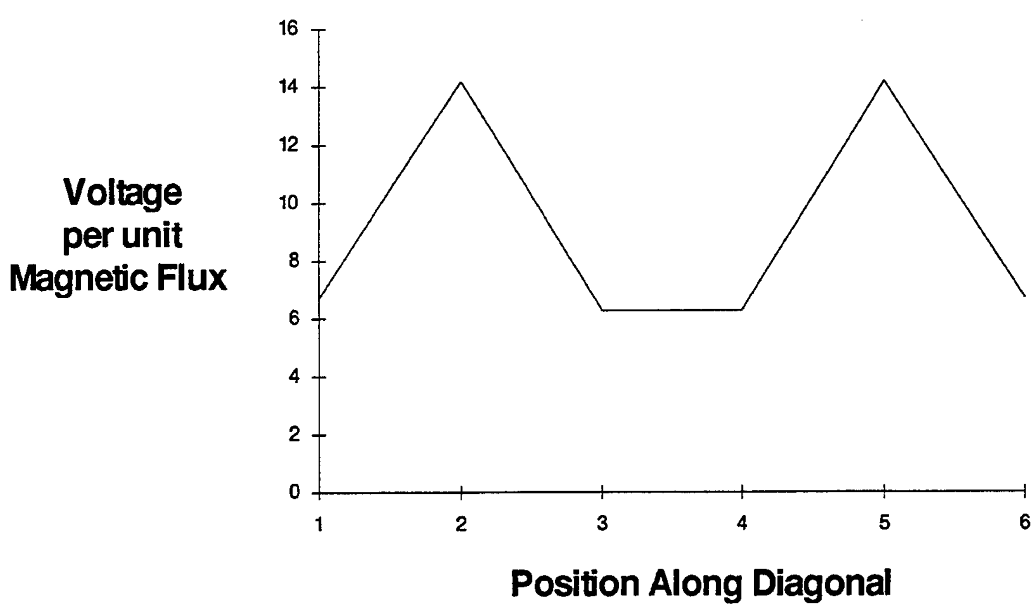

Figure 7. Plot of Main Diagonal Elements of Equation (2) for the Nondimensional Output of the Planar Grid Model's Computer Code for a 5 × 5 Grid Size.

$$\text{Output} = [\Lambda]_{r,s} = \frac{[v]_{r,s}}{\omega\phi_B} = \begin{bmatrix} 6.72 & 9.76 & 7.49 & 7.49 & 9.76 & 6.72 \\ 9.76 & 14.18 & 11.00 & 11.00 & 14.18 & 9.76 \\ 7.49 & 11.00 & 6.28 & 6.28 & 11.00 & 7.49 \\ 7.49 & 11.00 & 6.28 & 6.28 & 11.00 & 7.49 \\ 9.76 & 14.18 & 11.00 & 11.00 & 14.18 & 9.76 \\ 6.72 & 9.76 & 7.49 & 7.49 & 9.76 & 6.72 \end{bmatrix}, \tag{3}$$

where v_{rs} is the nodal voltage in volts at node (r,s), ω is the angular frequency, and ϕ_B is the magnetic flux in webers. Each number in equation (3) (output) represents the potential difference at each node of equation (2) (input). Note that some amount of voltage exists at each node and that the highest voltages occur at the corners of the polygon formed by the orthogonal tangents to the coil or flux region as shown in Figure 8. This distribution indicates that the nature of the thermal response in the laminate is dependent upon the size and shape of the coil and that the model's prediction is a function of the grid dimension used.

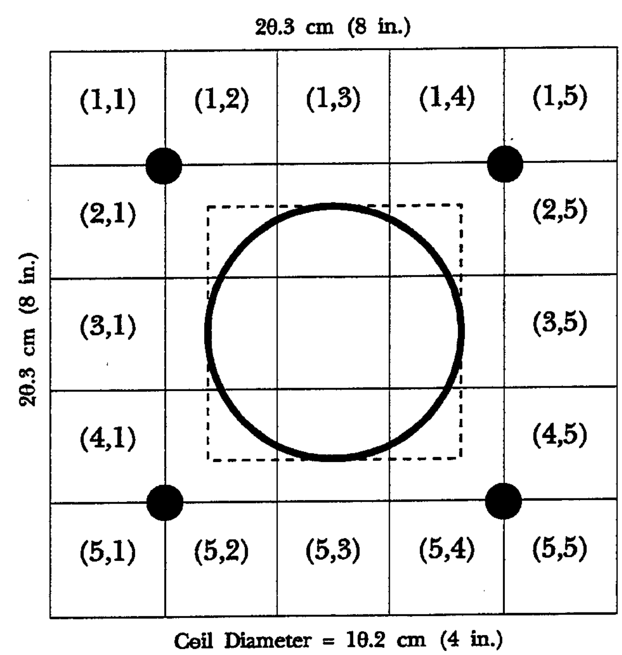

Figure 8. Prediction of the Points of Highest Heating for a 5 × 5 Grid Size Representation (Darkened Circles). In a Test Specimen, the Points of Highest Heating Fall at the Points of Intersection of the Tangents (Dashed Lines) to the Flux Region (Bold Circle) Due to the Nearly Infinitely Fine Grid.

4. Convergence Analysis

If $n_x x n_y$ is the size of the grid (i.e., $n_x = 5$, $n_y = 5$ in Figure 5), then the total number of loops possible is $1/4\ (n_x)(n_y)(n_x + 1)(n_y + 1)$. For a 5×5 grid, this represents 225 loops, and, for a 20×20 grid, 44,100 loops must be considered. Therefore, practical programing limitations on grid size exist. For example, a 20.3-cm-square (8 in) cross-ply specimen, such as that used in many of our experiments, would require approximately a $25{,}000 \times 25{,}000$ grid for exact representation. A convergence study was conducted to determine a minimum grid size required to achieve sufficiently accurate results. These grids were then used in further studies.

Square grid sizes ranging from $n_x = n_y = 3$ to 16 were studied. For this study, a coil-to-specimen area ratio of 14.2% was used. (With the coil centered on the specimen, the percentage of area covered by the coil and, thus, by the flux field was 14.2%.) Inputting a standardized unit flux, the amount of flux through each element could be determined as described earlier. This provided the input for each case studied. Figure 9 shows the superposition of diagonal potential distributions for five of the cases studied. The results are plotted as straight lines connecting the data points for ease of reading. A quantitative measure of the convergence is possible by comparing the volume under the surface plots for each case. This is equivalent to the average of all voltage values in the respective output matrices. Figure 10 shows these values plotted against the square grid size. Convergence occurs rather quickly, as shown again in Figure 11, where the percent error from the convergence value (8.6 in this example) is plotted against increasing grid size. Although this shows that a square grid size of 8 could be used with less than a 5% error, recall that this result is valid only when the area of the specimen surface covered by the coil is equal to or greater than 14.2%. Other considerations, such as the minimum number of grid elements or nodes covered by the coil, must be considered.

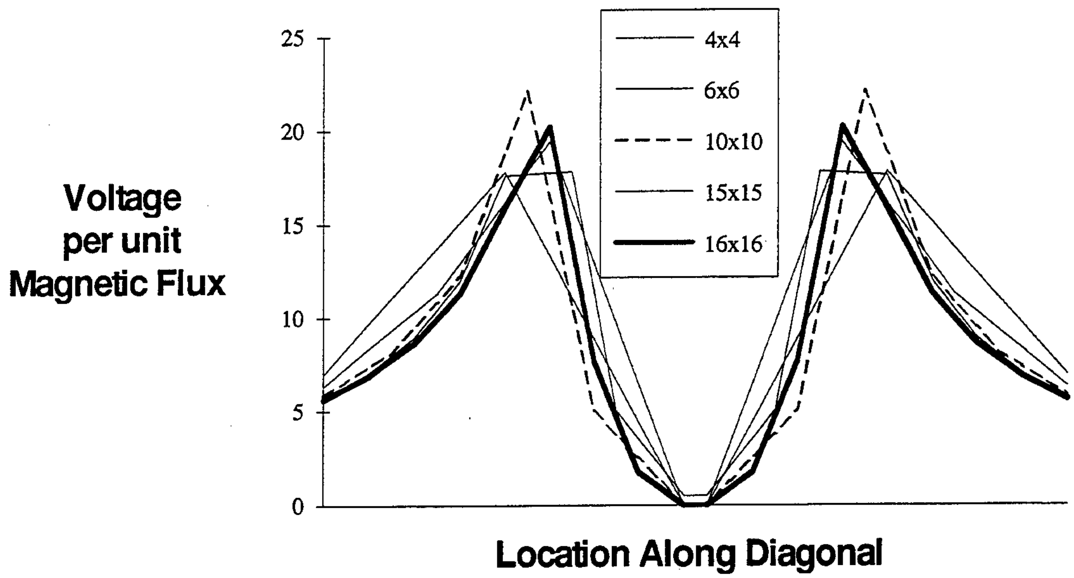

Figure 9. Superposition of Diagonal Nondimensional Voltage Distributions for Various Grid Densities From Planar Grid Model.

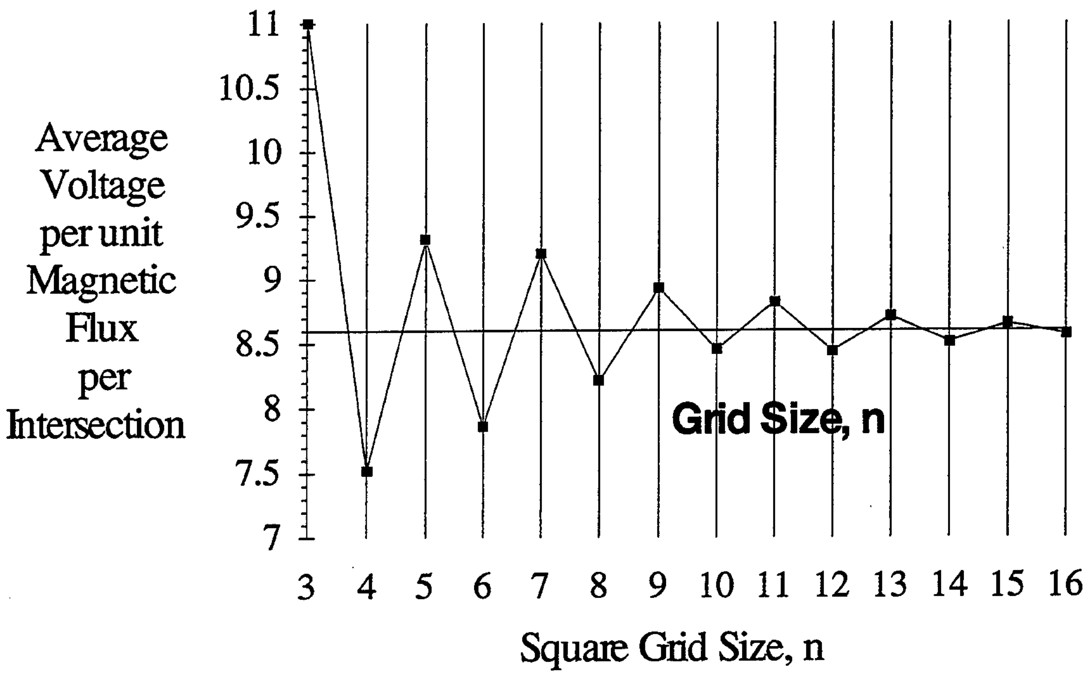

Figure 10. Plot of Average Nondimensional Voltage Values for Various Grid Densities From the Planar Grid Model. Note That the Horizontal Axis Is Placed at the Point of Convergence (8.6) on the Vertical Axis.

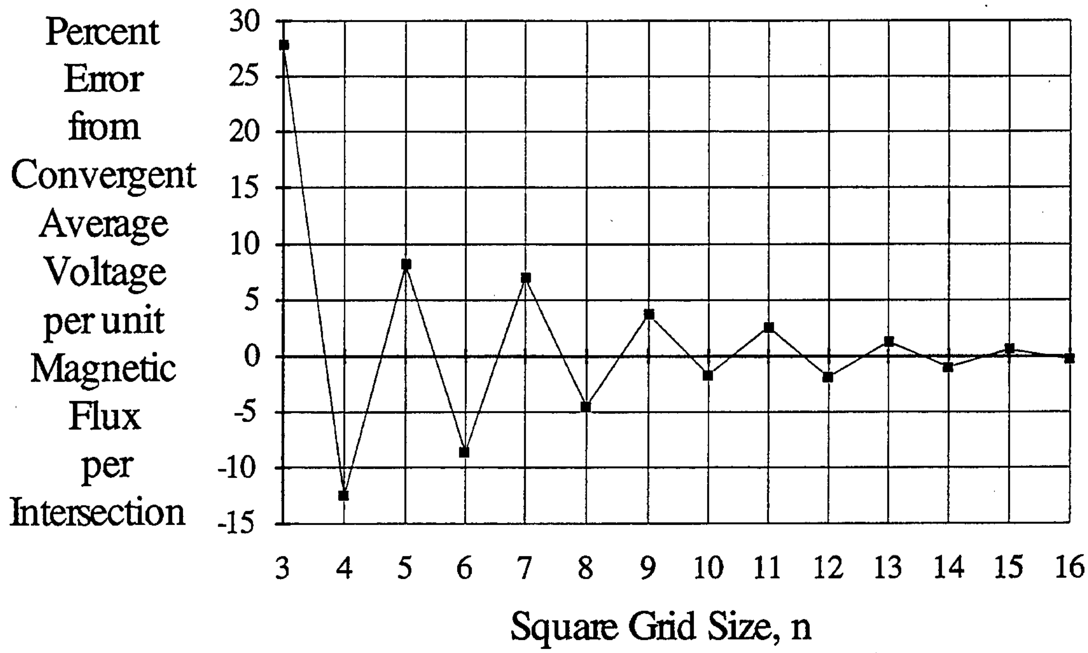

Figure 11. Plot of Percent Error of Average Nondimensional Voltage for Various Grid Sizes From the Convergent Solution at Infinite Grid Fineness. Note That an 8 × 8 Grid Size Is Within a 5% Error Limit From the Convergent Value Determined From Figure 10.

5. Parametric Analysis

5.1 Coil-to-Specimen Area Ratio. At one extreme where $A_{coil}/A_{specimen}$ is unity, the coil completely covers the cross-ply specimen. As usual, it is assumed that a homogenous magnetic field was produced by the Helmholtz coil. Grid sizes of 3 through 9 were studied for this situation. The percent differences (error values) are shown in Figure 12. Note that a grid size of 7 × 7 falls within our 5% error standard. (The maximum voltages for each grid size remained constant.) The convergence of the model at a fairly coarse grid size not only makes calculations faster but also validates the use of the model for representing the actual case of fibers forming a much finer mesh.

Figure 13 shows the results of applying a unit magnetic flux to various coil-to-specimen size ratios. In each case, the same total amount of flux is input to the specimen but the total nondimensional voltage is not constant. Figure 14 is a plot of the coil-to-specimen size ratio

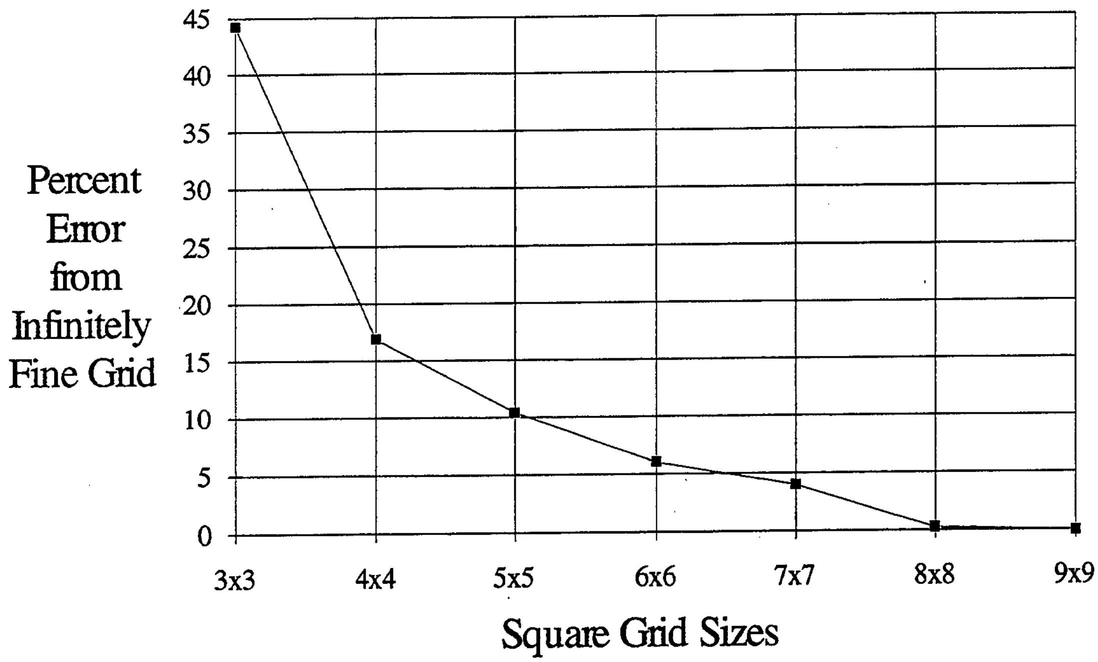

Figure 12. Results of Study to Determine Minimum Applicable Grid Size for the Situation in Which the Coil Completely Covers the Specimen (Coil-to-Specimen Area Ratio of Unity).

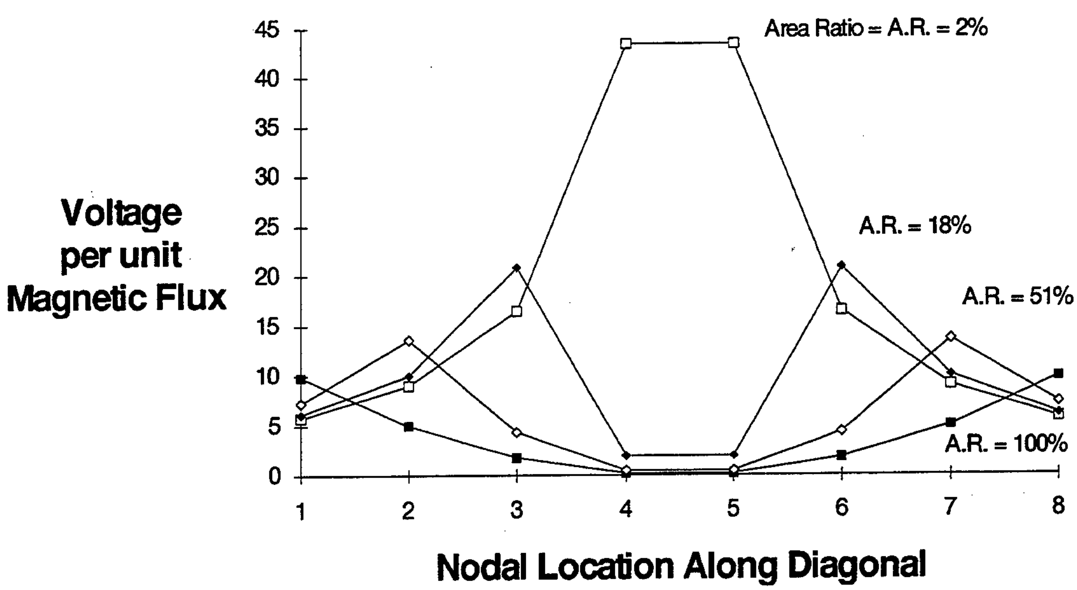

Figure 13. Predictions of the Effects of Changing the Size of the Helmholtz-Type Coil With Respect to the Size of the Laminate Specimen for Centered-Coil Experiments.

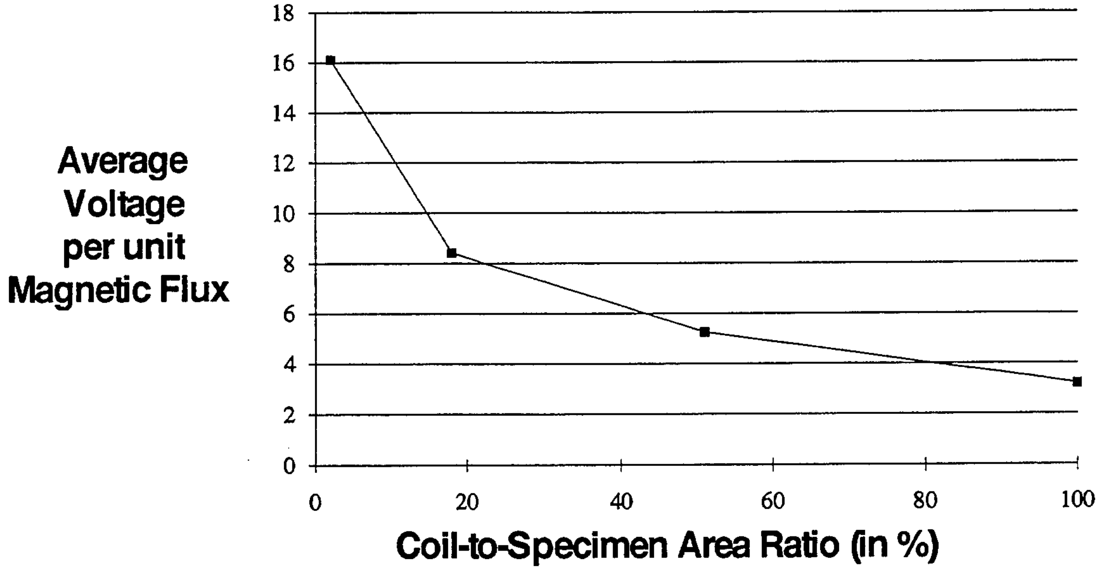

Figure 14. Averaged Results of Figure 13 Showing Decrease in Average Nondimensional Voltage With Increasing Size of Coil With Respect to the Specimen.

against the average nondimensional emf induced in the specimen. This result shows that increasing the area covered by the coil without increasing the total input flux decreases the total resulting emf energy. Conversely, localization of the flux in the plane increases both the total energy dissipated by the specimen and the gradients of heating in the plane.

5.2 Location of Coil. Three parametric studies were performed for a 6×6 grid with a coil that covered 14.2% of the grid surface. The coil is placed centered, shifted to an edge, and shifted to a corner, respectively, in the three cases. Figure 15 displays the three-dimensional (3-D) columnar plots for the three cases with their respective coil placements. Note that the location of the coil divides the total grid into four quadrants. If the coil is symmetrical, each quadrant has the same amount of energy induced, regardless of where the coil is placed. For example, moving the coil to a corner requires that one-fourth of the energy be dissipated in that corner.

Keeping the size of the coil and its energy constant, but moving it about in the plane of the specimen, changes both the average induced voltage and the maximum voltage value. The maximum energy is felt by the specimen when the coil is centered in the plane, and the minimum

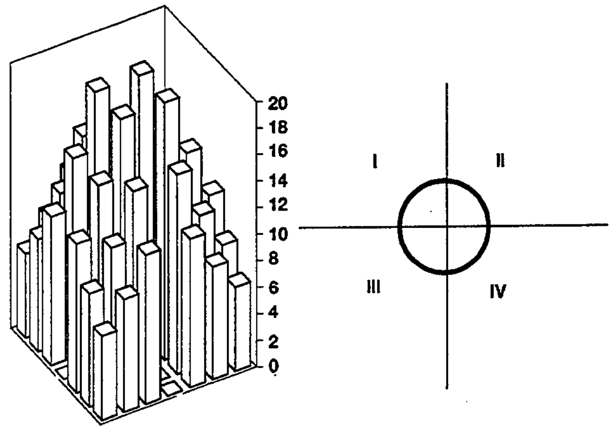

Centered Coil

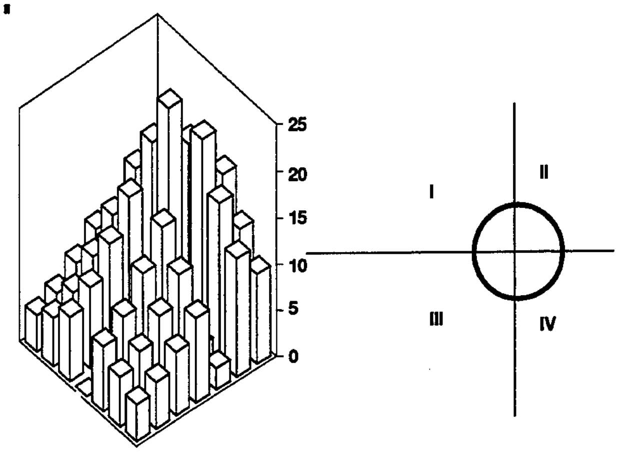

Coil Shifted to Edge

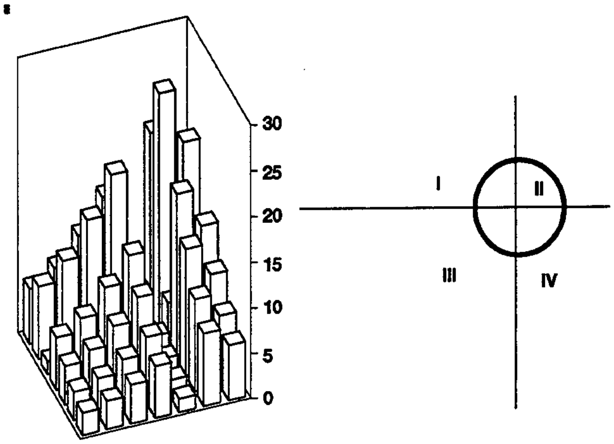

Coil Shifted to Corner

Figure 15. Predictions of Voltage per Unit Magnetic Flux for Varying the Location of the Helmholtz-Type Coil on a Cross-Ply Specimen. The Relative Size and Placement of the Coil Is Shown for Each Case. Note the Division of the Input Flux Into Four Equal Quadrants.

total energy is experienced when the coil is moved to a corner. For the slight shifts in coil position shown in Figure 15, the total energy disipated decreases 4% and 7.5% for the edge shift and corner shift, respectively. For a situation in which all the flux is forced into the corner element of the 6 × 6 grid, the decrease in energy dissipated is 44%. Note that the maximum voltage is still increased as the coil moves toward an edge (+16%) or corner (+3%). For the corner-point-flux case, the increase is 310%; however, this situation also involves decreasing the size of the coil with respect to the specimen. These observations explain the "edge and corner effects" described in the literature [3, 4].

The convergence of the model for square cross-ply specimens was examined at two coil-to-specimen area ratios: 14.2% and 100%. The results of these studies (Figures 11 and 12 respectively) indicate minimum grid sizes of 8 × 8 and 7 × 7, respectively, for errors of 5% from infinite grid fineness. It appears to be a reasonable assumption that, for any value of coil-to-specimen area ratio between 14% and 100%, the minimum square grid size would fall between 7 and 8, as shown in Figure 16.

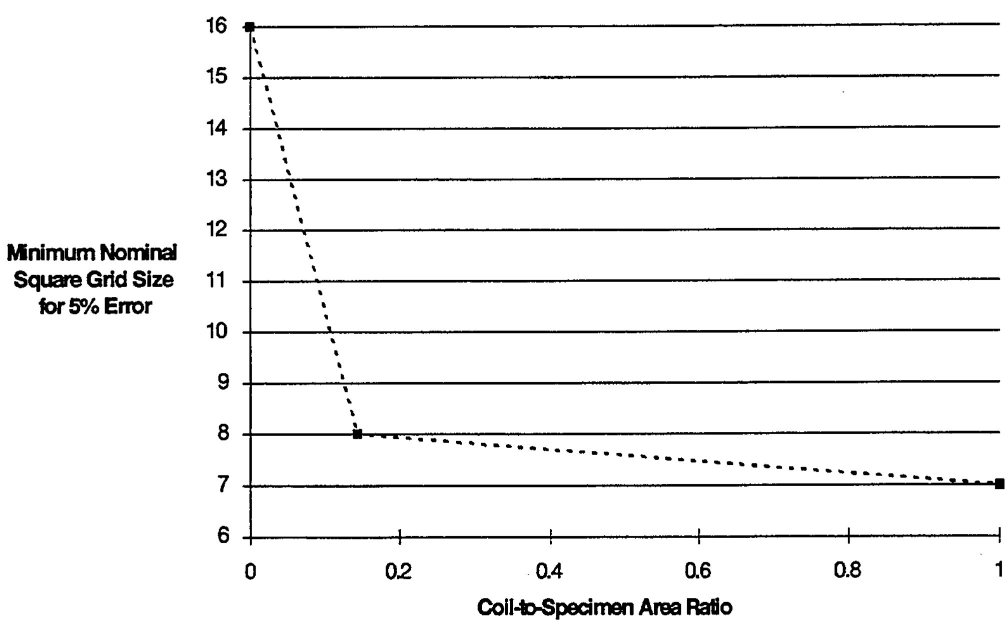

Figure 16. The "Accuracy Zone" for Coil-to-Specimen Size Ratio as It Relates to the Grid Density Used in the Planar Grid Model. Note That a Minimum Grid Size of 8 × 8 Is Accurate for All Coil-to-Specimen Area Ratios.

For coil sizes smaller than 14%, a steep increase in minimum grid size is expected. For example, consider a 20.3-cm-square (8 in) specimen with a 1.3-cm-diameter (0.5 in) coil. The coil-to-specimen area ratio is approximately 0.003. For the coil placed at the center of the specimen, a 16 × 16 grid size is necessary before any changes in the result occur since, for grid sizes coarser than 16 × 16, the coil diameter is less than the smallest conductive loop in the model. For square cross-ply specimens with centered coils, grid sizes of 7 or 8 are sufficiently accurate for coil-to-specimen area ratios greater than 14%.

6. Experimental Support

A 10 × 10 APC-2 tape grid was laid out between plates of glass, and a magnetic field was applied using the Helmholtz coil; each tape length was treated as a conductive element in the model. Figure 17 shows the tape layout, coil placement, and liquid-crystal thermal profile. The small circles represent the points of heating, as indicated by the liquid-crystal sheet in the 40–45°C range. The intensity of heating is thus indicated by the size of the dots. Note the four points of highest heating and the eight points of second-highest heating.

Figure 18 shows the 3-D mapping of the model's prediction, which coincides qualitatively with the experimental observation of Figure 17. Only the first two sets of "highest heating" are shown. All lower nondimensional voltages, representing values less than 60% of the maximum, are omitted for clarity.

A 20.3-cm-square (8 in) cross-ply AS4 graphite/PEEK $[0/90]_s$ laminated plate was examined using a 10.2-cm-diameter (4 in) Helmholtz coil placed at the center, edge, and corner of the specimen. Figure 19 displays the results of viewing 40–45°C liquid-crystal sheets during the heating. The prediction of heating for each case is given in Figure 15. A comparison of Figure 19, with predictions of Figure 15, indicates a close correlation between the planar voltage distribution and heating in the plane.

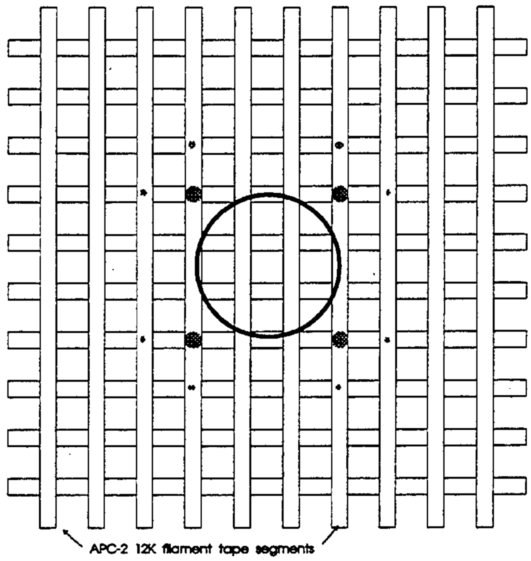

Figure 17. A 10 × 10 APC-2 Tape Grid. The Large Circle Represents the Placement of the Helmholtz Coil. The Small Circles Represent the Points of Heating as Indicated by Liquid Crystal Sheet (40–45°C Range). The Intensity of Heating Is Thus Indicated by the Size of the Dots. Note the Four Points of Highest Heating and the Eight Points of Second-Highest Heating.

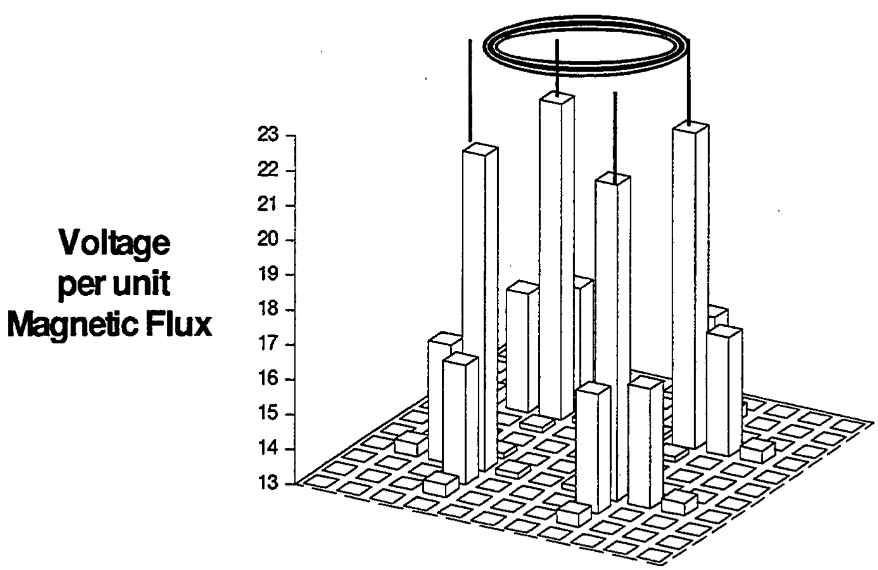

Figure 18. The Predicted Nondimensional Voltage Profile From the Planar Grid Model for the 10 × 10 Grid Representation Used to Model the Tape Segments of Figure 17. Only the First Two Sets of Highest Heating (Those in Excess of 13) Are Shown. All Lower Voltages Are Omitted Here for Clarity. The Ring Above the Graph Indicates the Placement of the Helmholtz Coil on the Specimen.

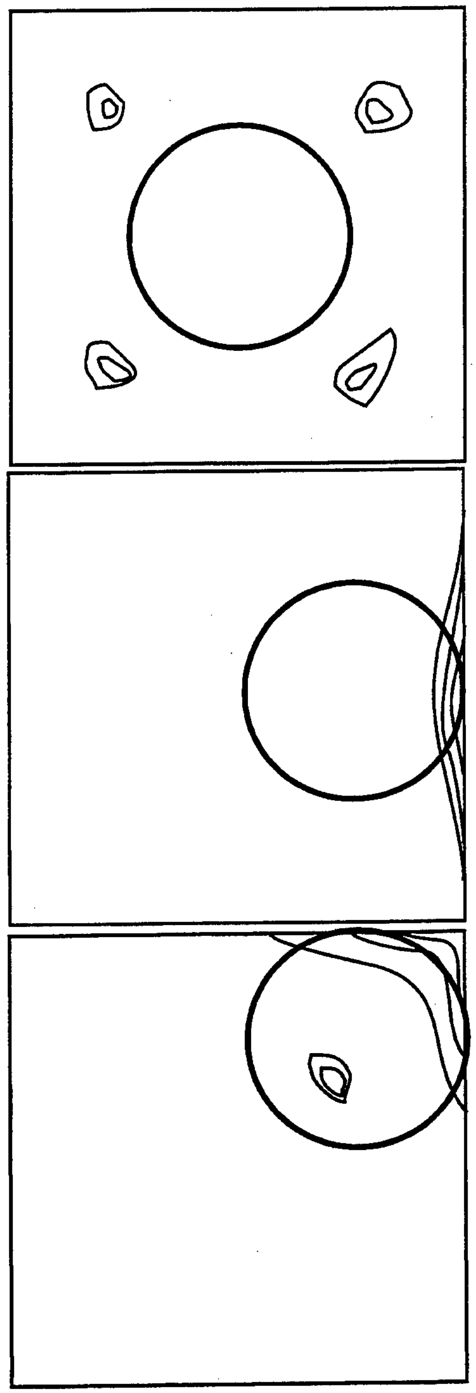

Figure 19. Results of Liquid-Crystal Thermal Measurement Observations for a 10-cm Helmholtz Coil on a 20-cm-square [0/90] Cross-Ply Laminate. The Ring Indicates the Placement of the Coil. The Contours Represent the Progression (From Inside To Outside) of Heating as Witnessed From the Liquid Crystal in the 40–45°C Range. Note the Points of Highest Heating, as Predicted in Figure 15.

7. Summary

A model to predict the distinct in-plane response of a continuous-carbon-fiber thermoplastic matrix cross-ply laminated composite plate to an alternating magnetic field has been developed. This model describes how the transversely applied magnetic field creates a rotational electrical potential field that induces a distribution of linear electric fields and nodal linear potential differences between crossing fibers in the plane of the cross-ply laminate. The planar grid model is represented by an algorithm that considers all the possible conductive loops in the planar system of crossing fibers by assuming a coarse grid density. The solution of this algorithm was shown to converge at a finite grid density, depending upon the size of the coil with respect to the specimen and upon the spatial placement of the coil on the specimen. The size and placement of the coil were also shown to significantly (and predictably) affect the strength and distribution of the electromagnetic response in the plane. This response was further shown to qualitatively predict the distribution of planar heat generation in the laminates. Experimental data from laminate surface temperature measurements using liquid-crystal sheets compared well qualitatively with the theory. As a result of this study, a fundamental understanding of the controlling mechanisms of thermal generation in continuous-carbon-fiber systems under the influence of an alternating magnetic field is established.

In order to correlate this planar electric potential distribution to thermal generation, it is necessary to model the mechanisms of field distribution through the thickness. The information presented in this work can be refined by taking into account the through-thickness response (i.e., How do the nodal voltages between fibers in adjacent orthogonal plies, obtained from the planar grid model, interact with each other to establish linear electric fields in the interfiber polymeric regions?). This requirement is accomplished through the fiber layer submodel to be presented in a separate communication.

The planar grid model and the supporting experimental evidence address a new complexity to the issue of joining and field repair of thermoplastic-based composites by magnetic induction heating. The possibility of extreme gradients of heat generation in the plane of these materials demands further research in this area.

INTENTIONALLY LEFT BLANK.

8. References

1. Fink, B. K., R. L. McCullough, and J. W. Gillespie, Jr. "A Local Theory of Heating in Cross-Ply Carbon Fiber Thermoplastic Composites by Magnetic Induction." *Polymer Engineering and Science*, vol. 32, no. 5, 357–369, 1992.

2. Fink, B. K. "Heating of Continuous-Carbon-Fiber Thermoplastic-Matrix Composites by Magnetic Induction." Ph.D. dissertation, University of Delaware, 1991.

3. Border, J., and R. Salas. "Induction Heated Joining of Thermoplastic Composites Without Metal Susceptors." *34th SAMPE Symposium,* 1989.

4. Border, J. "Understanding Induction Heating and Its Utilization for Aircraft Structural Repair." Contract No. F33657-88-C-0087: PDA-89-FR-5865-00-2, PDA Engineering, Final Report for McDonnell Aircraft Co., 1989.

INTENTIONALLY LEFT BLANK.

NO. OF COPIES	ORGANIZATION
2	DEFENSE TECHNICAL INFORMATION CENTER DTIC DDA 8725 JOHN J KINGMAN RD STE 0944 FT BELVOIR VA 22060-6218
1	HQDA DAMO FDQ D SCHMIDT 400 ARMY PENTAGON WASHINGTON DC 20310-0460
1	OSD OUSD(A&T)/ODDDR&E(R) R J TREW THE PENTAGON WASHINGTON DC 20301-7100
1	DPTY CG FOR RDA US ARMY MATERIEL CMD AMCRDA 5001 EISENHOWER AVE ALEXANDRIA VA 22333-0001
1	INST FOR ADVNCD TCHNLGY THE UNIV OF TEXAS AT AUSTIN PO BOX 202797 AUSTIN TX 78720-2797
1	DARPA B KASPAR 3701 N FAIRFAX DR ARLINGTON VA 22203-1714
1	NAVAL SURFACE WARFARE CTR CODE B07 J PENNELLA 17320 DAHLGREN RD BLDG 1470 RM 1101 DAHLGREN VA 22448-5100
1	US MILITARY ACADEMY MATH SCI CTR OF EXCELLENCE DEPT OF MATHEMATICAL SCI MADN MATH THAYER HALL WEST POINT NY 10996-1786

NO. OF COPIES	ORGANIZATION
1	DIRECTOR US ARMY RESEARCH LAB AMSRL DD J J ROCCHIO 2800 POWDER MILL RD ADELPHI MD 20783-1197
1	DIRECTOR US ARMY RESEARCH LAB AMSRL CS AS (RECORDS MGMT) 2800 POWDER MILL RD ADELPHI MD 20783-1145
3	DIRECTOR US ARMY RESEARCH LAB AMSRL CI LL 2800 POWDER MILL RD ADELPHI MD 20783-1145
	<u>ABERDEEN PROVING GROUND</u>
4	DIR USARL AMSRL CI LP (BLDG 305)

NO. OF COPIES	ORGANIZATION
1	DIRECTOR USARL AMSRL CP CA D SNIDER 2800 POWDER MILL RD ADELPHI MD 20783
1	COMMANDER USA ARDEC AMSTA AR FSE T GORA PICATINNY ARSENAL NJ 07806-5000
3	COMMANDER USA ARDEC AMSTA AR TD PICATINY ARSENAL NJ 078806-5000
5	COMMANDER USA TACOM AMSTA JSK S GOODMAN J FLORENCE AMSTA TR D B RAJU L HINOJOSA D OSTBERG WARREN MI 48397-5000
5	PM SADARM SFAE GCSS SD COL B ELLIS M DEVINE W DEMASSI J PRITCHARD S HROWNAK PICATINNY ARSENAL NJ 07806-5000
1	COMMANDER USA ARDEC F MCLAUGHLIN PICATINNY ARSENAL NJ 07806-5000

NO OF. COPIES	ORGANIZATION
5	COMMANDER USA ARDEC AMSTA AR CCH S MUSALLI R CARR M LUCIANO T LOUCEIRO PICATINNY ARSENAL NJ 07806-5000
4	COMMANDER USA ARDEC AMSTA AR (2CPS) E FENNEL (2 CPS) PICATINNY ARSENAL NJ 07806-5000
1	COMMANDER USA ARDEC AMSTA AR CCH P J LUTZ PICATINNY ARSENAL NJ 07806-5000
1	COMMANDER USA ARDEC AMSTA AR FSF T C LIVECCHIA PICATINNY ARSENAL NJ 07806-5000
1	COMMANDER USA ARDEC AMSTA AR QAC T/C C PATEL PICATINNY ARSENAL NJ 07806-5000
2	COMMANDER USA ARDEC AMSTA AR M D DEMELLA F DIORIO PICATINNY ARSENAL NJ 07806-5000

NO. OF COPIES	ORGANIZATION
3	COMMANDER USA ARDEC AMSTA AR FSA A WARNASH B MACHAK M CHIEFA PICATINNY ARSENAL NJ 07806-5000
1	COMMANDER SMCWV QAE Q B VANINA BLDG 44 WATERVLIET ARSENAL WATERVLIET NY 12189-4050
1	COMMANDER SMCWV SPM T MCCLOSKEY BLDG 253 WATERVLIET ARSENAL WATERVLIET NY 12189-4050
8	DIRECTORECTOR BENET LABORATORIES AMSTA AR CCB J KEANE J BATTAGLIA J VASILAKIS G FFIAR V MONTVORI G DANDREA R HASENBEIN AMSTA AR CCB R S SOPOK WATERVLIET NY 12189-4050
1	COMMANDER SMCWV QA QS K INSCO WATERVLIET NY 12189-4050
1	COMMANDER PRODUCTION BASE MODERN ACTY USA ARDEC AMSMC PBM K PICATINNY ARSENAL NJ 07806-5000

NO OF. COPIES	ORGANIZATION
1	COMMANDER USA BELVOIR RD&E CTR STRBE JBC FT BELVOIR VA 22060-5606
2	COMMANDER USA ARDEC AMSTA AR FSB G M SCHIKSNIS D CARLUCCI PICATINNY ARSENAL NJ 07806-5000
1	US ARMY COLD REGIONS RESEARCH & ENGINEERING CTR P DUTTA 72 LYME RD HANVOVER NH 03755
1	DIRECTOR USARL AMSRL WT L D WOODBURY 2800 POWDER MILL RD ADELPHI MD 20783-1145
1	COMMANDER USA MICOM AMSMI RD W MCCORKLE REDSTONE ARSENAL AL 35898-5247
1	COMMANDER USA MICOM AMSMI RD ST P DOYLE REDSTONE ARSENAL AL 35898-5247
1	COMMANDER USA MICOM AMSMI RD ST CN T VANDIVER REDSTONE ARSENAL AL 35898-5247
3	US ARMY RESEARCH OFFICE A CROWSON K LOGAN J CHANDRA PO BOX 12211 RESEARCH TRIANGLE PARK NC 27709-2211

NO. OF COPIES	ORGANIZATION
3	US ARMY RESEARCH OFFICE ENGINEERING SCIENCES DIV R SINGLETON G ANDERSON K IYER PO BOX 12211 RESEARCH TRIANGLE PARK NC 27709-2211
5	PM TMAS SFAE GSSC TMA COL PAWLICKI K KIMKER E KOPACZ R ROESER B DORCY PICATINNY ARSENAL NJ 07806-5000
1	PM TMAS SFAE GSSC TMA SMD R KOWALSKI PICATINNY ARSENAL NJ 07806-5000
3	PEO FIELD ARTILLERY SYSTEMS SFAE FAS PM H GOLDMAN T MCWILLIAMS T LINDSAY PICATINNY ARSENAL NJ 07806-5000
2	PM CRUSADER G DELCOCO J SHIELDS PICATINNY ARSENAL NJ 07806-5000
3	NASA LANGLEY RESEARCH CTR MS 266 AMSRL VS W ELBER F BARTLETT JR C DAVILA HAMPTON VA 23681-0001

NO OF. COPIES	ORGANIZATION
2	COMMANDER DARPA S WAX 2701 N FAIRFAX DR ARLINGTON VA 22203-1714
6	COMMANDER WRIGHT PATTERSON AFB WL FIV A MAYER WL MLBM S DONALDSON T BENSON-TOLLE C BROWNING J MCCOY F ABRAMS 2941 P ST STE 1 DAYTON OH 45433
2	NAVAL SURFACE WARFARE CTR DAHLGREN DIV CODE G06 R HUBBARD CODE G 33 C DAHLGREN VA 22448
1	NAVAL RESEARCH LAB I WOLOCK CODE 6383 WASHINGTON DC 20375-5000
1	OFFICE OF NAVAL RESEARCH MECH DIV Y RAJAPAKSE CODE 1132SM ARLINGTON VA 22271
1	NAVAL SURFACE WARFARE CTR CRANE DIV M JOHNSON CODE 20H4 LOUISVILLE KY 40214-5245
1	DAVID TAYLOR RESEARCH CTR SHIP STRUCTURES & PROTECTION DEPT J CORRADO CODE 1702 BETHESDA MD 20084
2	DAVID TAYLOR RESEARCH CTR R ROCKWELL W PHYILLAIER BETHESDA MD 20054-5000

NO. OF COPIES	ORGANIZATION
1	DEFENSE NUCLEAR AGENCY INNOVATIVE CONCEPTS DIV R ROHR 6801 TELEGRAPH RD ALEXANDRIA VA 22310-3398
1	EXPEDITIONARY WARFARE DIV N85 F SHOUP 2000 NAVY PENTAGON WASHINGTON DC 20350-2000
1	OFFICE OF NAVAL RESEARCH D SIEGEL 351 800 N QUINCY ST ARLINGTON VA 22217-5660
7	NAVAL SURFACE WARFARE CTR J H FRANCIS CODE G30 D WILSON CODE G32 R D COOPER CODE G32 E ROWE CODE G33 T DURAN CODE G33 L DE SIMONE CODE G33 DAHLGREN VA 22448
1	COMMANDER NAVAL SEA SYSTEM CMD P LIESE 2351 JEFFERSON DAVIS HIGHWAY ARLINGTON VA 22242-5160
1	NAVAL SURFACE WARFARE CTR M E LACY CODE B02 17320 DAHLGREN RD DAHLGREN VA 22448
1	NAVAL WARFARE SURFACE CTR TECH LIBRARY CODE 323 17320 DAHLGREN RD DAHLGREN VA 22448
4	DIR LLNL R CHRISTENSEN S DETERESA F MAGMESS M FINGER PO BOX 808 LIVERMORE CA 94550

NO OF. COPIES	ORGANIZATION
2	DIRECTOR LLNL F ADDESSIO MS B216 J REPPA MS F668 PO BOX 1633 LOS ALAMOS NM 87545
3	UNITED DEFENSE LP 4800 EAST RIVER DR P JANKE MS170 T GIOVANETTI MS236 B VAN WYK MS 389 MINNEAPOLIS MN 55421-1498
4	DIRECTOR SANDIA NATIONAL LAB APPLIED MECHANICS DEPT DIV 8241 W KAWAHARA K PERANO D DAWSON P NIELAN PO BOX 969 LIVERMORE CA 94550-0096
1	BATTALLE C R HARGREAVES 505 KNIG AVE COLUMBUS OH 43201-2681
1	PACIFIC NORTHWEST LAB M SMITH PO BOX 999 RICHLAND WA 99352
1	LLNL M MURPHY PO BOX 808 L 282 LIVERMORE CA 94550
10	UNIV OF DELAWARE CTR FOR OCMPOSITE MATERIALS J GILLESPIE 201 SPENCER LAB NEWARK DE 19716

NO. OF COPIES	ORGANIZATION
2	THE U OF TEXAS AT AUSTIN CTR ELECTROMECHANICS A WALLIS J KITZMILLER 10100 BURNET RD AUSTIN TX 78758-4497
1	AAI CORPORATION T G STASTNY PO BOX 126 HUNT VALLEY MD 21030-0126
1	SAIC D DAKIN 2200 POWELL ST STE 1090 EMERYVILLE CA 94608
1	SAIC M PALMER 2109 AIR PARK RD S E ALBUQUERQUE NM 87106
1	SAIC R ACEBAL 1225 JOHNSON FERRY RD STE 100 MARIETTA GA 30068
1	SAIC G CHRYSSOMALLIS 3800 W 80TH ST STE 1090 BLOOMINGTON MN 55431
6	ALLIANT TECHSYSTEMS INC C CANDLAND R BECKER L LEE R LONG D KAMDAR G KASSUELKE 600 2ND ST NE HOPKINS MN 55343-8367
1	CUSTOM ANALYTICAL ENGR SYS INC A ALEXANDER 13000 TENSOR LANE NE FLINTSTONE MD 21530

NO OF. COPIES	ORGANIZATION
1	NOESIS INC 1110 N GLEBE RD STE 250 ARLINGTON VA 22201-4795
1	ARROW TECH ASSO 1233 SHELBURNE RD STE D 8 SOUTH BURLINGTON VT 05403-7700
5	GEN CORP AEROJET D PILLASCH T COULTER C FLYNN D RUBAREZUL M GREINER 1100 WEST HOLLYVALE ST AZUSA CA 91702-0296
1	NIST STRUCTURE & MECHANICS GRP POLYMER DIV POLYMERS RM A209 G MCKENNA GAITHERSBURG MD 20899
1	GENERAL DYNAMICS LAND SYSTEM DIVISION D BARTLE PO BOX 1901 WARREN MI 48090
4	INSTITUTE FOR ADVANCED TECHNOLOGY H FAIR P SULILVAN W REINECKE I MCNAB 4030 2 W BRAKER LN AUSTIN TX 78759
1	PM ADVANCED CONCEPTS LORAL VOUGHT SYSTEMS J TAYLOR MS WT 21 PO BOX 650003 DALLAS TX 76265-0003

NO. OF COPIES	ORGANIZATION
2	UNITED DEFENSE LP P PARA G THOMASA 1107 COLEMAN AVE BOX 367 SAN JOSE CA 95103
1	MARINE CORPS SYSTEMS CMD PM GROUND WPNS COL R OWEN 2083 BARNETT AVE STE 315 QUANTICO VA 22134-5000
1	OFFICE OF NAVAL RES J KELLY 800 NORTH QUINCEY ST ARLINGTON VA 22217-5000
1	NAVSEE OJRI G CAMPONESCHI 2351 JEFFERSON DAVIS HWY ARLINGTON VA 22242-5160
1	USAF WL MLS O L A HAKIM 5525 BAILEY LOOP 243E MCCLELLAN AFB CA 55552
1	NASA LANGLEY J MASTERS MS 389 HAMPTON VA 23662-5225
2	FAA TECH CTR D OPLINGER AAR 431 P SHYPRYKEVICH AAR 431 ATLANTIC CITY NJ 08405
1	NASA LANGLEY RC CC POE MS 188E NEWPORT NEWS VA 23608
1	USAF WL MLBC E SHINN 2941 PST STE 1 WRIGHT PATTERSON AFB OH 45433-7750

NO OF. COPIES	ORGANIZATION
4	NIST POLYMERS DIVISION R PARNAS J DUNKERS M VANLANDINGHAM D HUNSTON GAITHERSBURG MD 20899
1	OAK RIDGE NATIONAL LAB A WERESZCZAK BLDG 4515 MS 6069 PO BOX 2008 OAKRIDGE TN 37831-6064
1	COMMANDER USA ARDEC INDUSTRIAL ECOLOGY CTR T SACHAR BLDG 172 PICATINNY ARSENAL NJ 07806-5000
1	COMMANDER USA ATCOM AVIATION APPLIED TECH DIR J SCHUCK FT EUSTIS VA 23604
1	COMMANDER USA ARDEC AMSTA AR SRE D YEE PICATINNY ARSENAL NJ 07806-5000
1	COMMANDER USA ARDEC AMSTA AR QAC T D RIGOGLIOSO BLDG 354 M829E3 IPT PICATINNY ARSENAL NJ 07806-5000

NO. OF COPIES	ORGANIZATION
7	COMMANDER USA ARDEC AMSTA AR CCH B B KONRAD E RIVERA G EUSTICE S PATEL G WAGNECZ R SAYER F CHANG BLDG 65 PICATINNY ARSENAL NJ 07806-5000
6	DIRECTOR US ARMY RESEARCH LAB AMSRL WM MB A ABRAHAMIAN M BERMAN A FRYDMAN T LI W MCINTOSH E SZYMANSKI 2800 POWDER MILL RD ADELPHI MD 20783-1197

ABERDEEN PROVING GROUND

NO. OF COPIES	ORGANIZATION
67	DIR USARL AMSRL CI AMSRL CI C W STUREK AMSRL CI CB R KASTE AMSRL CI S A MARK AMSRL SL B AMSRL SL BA AMSRL SL BE D BELY AMSRL WM B A HORST E SCHMIDT AMSRL WM BE G WREN C LEVERITT D KOOKER AMSRL WM BC P PLOSTINS D LYON J NEWILL AMSRL WM BD S WILKERSON R FIFER B FORCH R PESCE RODRIGUEZ B RICE AMSRL WM D VIECHNICKI G HAGNAUER J MCCAULEY AMSRL WM MA R SHUFORD S MCKNIGHT L GHIORSE AMSRL WM MB V HARIK J SANDS W DRYSDALE J BENDER T BLANAS T BOGETTI R BOSSOLI L BURTON S CORNELISON P DEHMER R DOOLEY B FINK G GAZONAS S GHIORSE D GRANVILLE D HOPKINS C HOPPEL D HENRY R KASTE M LEADORE R LIEB E RIGAS D SPAGNUOLO W SPURGEON J TZENG AMSRL WM MC J BEATTY AMSRL WM MD W ROY AMSRL WM T B BURNS

NO. OF COPIES	ORGANIZATION
	ABERDEEN PROVING GROUND (CONT)
	AMSRL WM TA W GILLICH E RAPACKI T HAVEL AMSRL WM TC R COATES W DE ROSSET AMSRL WM TD W BRUCHEY A D GUPTA AMSRL WM BB H ROGERS AMSRL WM BA F BRANDON W D AMICO AMSRL WM BR J BORNSTEIN AMSRL WM TE A NIILER AMSRL WM BF J LACETERA

INTENTIONALLY LEFT BLANK.

REPORT DOCUMENTATION PAGE

Form Approved
OMB No. 0704-0188

Public reporting burden for this collection of information is estimated to average 1 hour per response, including the time for reviewing instructions, searching existing data sources, gathering and maintaining the data needed, and completing and reviewing the collection of information. Send comments regarding this burden estimate or any other aspect of this collection of information, including suggestions for reducing this burden, to Washington Headquarters Services, Directorate for Information Operations and Reports, 1215 Jefferson Davis Highway, Suite 1204, Arlington, VA 22202-4302, and to the Office of Management and Budget, Paperwork Reduction Project(0704-0188), Washington, DC 20503.

1. AGENCY USE ONLY *(Leave blank)*

2. REPORT DATE
November 1999

3. REPORT TYPE AND DATES COVERED
Final, Dec 94 - Mar 96

4. TITLE AND SUBTITLE
Induction Heating of Carbon-Fiber Composites: Electrical Potential Distribution Model

5. FUNDING NUMBERS
AH42

6. AUTHOR(S)
Bruce K. Fink, Roy L. McCullough,* and John W. Gillespie Jr.*

7. PERFORMING ORGANIZATION NAME(S) AND ADDRESS(ES)
U.S. Army Research Laboratory
ATTN: AMSRL-WM-MB
Aberdeen Proving Ground, MD 21005-5069

8. PERFORMING ORGANIZATION REPORT NUMBER
ARL-TR-2130

9. SPONSORING/MONITORING AGENCY NAMES(S) AND ADDRESS(ES)

10. SPONSORING/MONITORING AGENCY REPORT NUMBER

11. SUPPLEMENTARY NOTES
*University of Delaware, Newark, DE 19716

12a. DISTRIBUTION/AVAILABILITY STATEMENT
Approved for public release; distribution is unlimited.

12b. DISTRIBUTION CODE

13. ABSTRACT *(Maximum 200 words)*
Mechanisms of heat generation and distribution in carbon-fiber-based composites subjected to an alternating magnetic field are considered. A model that predicts the strength and distribution of these heat sources in the plane of the cross-ply laminate configurations has been developed and verified. In this analysis, the fibers in a cross-ply pair are treated as a grid of conductive loops in the plane. Each such conductive loop uses the alternating magnetic field to produce a rotational electromotive force that induces electric fields in the polymeric regions. Induced electromagnetic energy is converted into thermal energy through dielectric losses in polymeric regions between the carbon fibers in the adjacent orthogonal plies that the conductive loops comprise. Each possible conductive loop is accounted for, and the resulting superposition of potential differences at the nodes leads to the in-plane profile of the electric field in the polymeric regions. Data from AS4 graphite-reinforced polyetheretherketone (PEEK) laminate surface temperature measurements using liquid crystal sheets compare qualitatively with the theory.

14. SUBJECT TERMS
carbon filter, induction heating, composites, dielectric properties

15. NUMBER OF PAGES
37

16. PRICE CODE

17. SECURITY CLASSIFICATION OF REPORT	18. SECURITY CLASSIFICATION OF THIS PAGE	19. SECURITY CLASSIFICATION OF ABSTRACT	20. LIMITATION OF ABSTRACT
UNCLASSIFIED	UNCLASSIFIED	UNCLASSIFIED	UL

NSN 7540-01-280-5500

Standard Form 298 (Rev. 2-89)
Prescribed by ANSI Std. 239-18 298-102

INTENTIONALLY LEFT BLANK.

USER EVALUATION SHEET/CHANGE OF ADDRESS

This Laboratory undertakes a continuing effort to improve the quality of the reports it publishes. Your comments/answers to the items/questions below will aid us in our efforts.

1. ARL Report Number/Author ARL-TR-2130 (Fink) Date of Report November 1999

2. Date Report Received ______

3. Does this report satisfy a need? (Comment on purpose, related project, or other area of interest for which the report will be used.) ______

4. Specifically, how is the report being used? (Information source, design data, procedure, source of ideas, etc.) ______

5. Has the information in this report led to any quantitative savings as far as man-hours or dollars saved, operating costs avoided, or efficiencies achieved, etc? If so, please elaborate. ______

6. General Comments. What do you think should be changed to improve future reports? (Indicate changes to organization, technical content, format, etc.) ______

CURRENT ADDRESS

Organization

Name E-mail Name

Street or P.O. Box No.

City, State, Zip Code

7. If indicating a Change of Address or Address Correction, please provide the Current or Correct address above and the Old or Incorrect address below.

OLD ADDRESS

Organization

Name

Street or P.O. Box No.

City, State, Zip Code

(Remove this sheet, fold as indicated, tape closed, and mail.)

(DO NOT STAPLE)